JLAB-TH-..., YITP-SB-2021-...

Neutrino-tagged jets at the Electron-Ion Collider

Miguel Arratia,[1] Zhong-Bo Kang,[2,3,4] Sebouh J. Paul,[1] Alexei Prokudin,[5,6] Felix Ringer,[7,8,9,6] and Fanyi Zhao[2,3,4]

[1] *Department of Physics and Astronomy, University of California, Riverside, CA 92521, USA*
[2] *Department of Physics and Astronomy, University of California, Los Angeles, CA 90095, USA*
[3] *Mani L. Bhaumik Institute for Theoretical Physics, University of California, Los Angeles, CA 90095, USA*
[4] *Center for Frontiers in Nuclear Science, Stony Brook University, Stony Brook, NY 11794, USA*
[5] *Division of Science, Penn State University Berks, Reading, PA 19610, USA*
[6] *Thomas Jefferson National Accelerator Facility, Newport News, VA 23606, USA*
[7] *C.N. Yang Institute for Theoretical Physics, Stony Brook University, Stony Brook, NY 11794,USA*
[8] *Department of Physics and Astronomy, Stony Brook University, Stony Brook, NY 11794, USA*
[9] *Department of Physics, Old Dominion University, Norfolk, VA 23529, USA*

(Dated: November 17, 2022)

We explore the potential of jet observables in charged-current deep-inelastic scattering (DIS) events at the future Electron-Ion Collider (EIC). Tagging jets with a recoiling neutrino, which can be identified with the event's missing transverse energy, will allow for flavor-sensitive measurements of transverse-momentum dependent parton density functions. We present the first predictions for transverse-spin asymmetries in azimuthal neutrino-jet correlations which probe the Sivers effect. We project the kinematic reach and the precision of these measurements and study their feasibility using parametrized detector simulations. We conclude that jet production in charged-current DIS, while challenging in terms of luminosity requirements, can complement the EIC 3D imaging program.

I. INTRODUCTION

The Electron-Ion Collider(EIC) will usher in a new era for the study of the 3D structure of the nucleon [1, 2]. Its high luminosity and polarization of both electron and hadron beams will enable precise measurements of spin and transverse-momentum-dependent (TMD) structure functions.

The EIC will produce the first jets in deep-inelastic scattering (DIS) off transversely-polarized nucleons. The potential of jets produced in neutral-current (NC) DIS has been explored extensively, e.g. in Refs. [3–11]. In this work, we focus on jets produced in charged-current (CC) DIS.

The CC DIS channel, which involves the exchange of a virtual W boson, leads to a quark-flavor sensitivity of jet measurements. The leading-order process, $W^* q \to q'$, is illustrated in Fig. I. Due to the conservation of electrical charge, electrons can only scatter via W^- off positively charged partons, which are predominantly u quarks, especially at large x. Likewise, with a positron beam, one can select scattering predominantly from d quarks through W^+ exchange. Moreover, tagging either charm or strange jets can further enhance the flavor sensitivity.

The H1 and ZEUS collaborations measured inclusive CC DIS off protons with longitudinally polarized electron and positron beams [12–17]. These measurements constrained the flavor dependence of collinear parton distribution functions (PDFs) [18]. Moreover, jet production in CC DIS was measured by the ZEUS collaboration [19, 20], and compared to next-to-next-to-next-to-leading order QCD calculations [21].

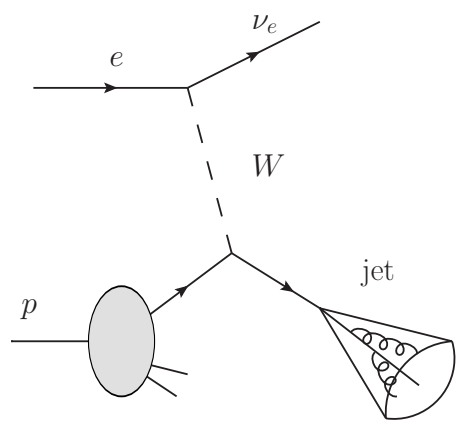

Figure 1. Charged-current DIS where the produced jet recoils against a neutrino.

One of the main challenges in measuring CC DIS is the measurement of the events' kinematic variables x and Q^2 in the presence of a final-state neutrino. Several methods were developed at the HERA to overcome this challenge [13, 22]. Feasibility studies of CC DIS at the EIC have been performed in Refs. [2, 23] for DIS off longitudinally-polarized protons with the goal to access

helicity PDFs; here we focus on TMDs and transverse-spin effects.

In SIDIS, transverse-spin asymmetries are extracted from modulations of the azimuthal angle with respect to the virtual-boson direction, typically in the Breit frame [24–27]. In CC DIS, this approach requires a measurement of the 3-momentum of the scattered neutrino to define the azimuthal angle, which is challenging due to acceptance losses at forward angles.

Jet-based measurements of spin asymmetries can reduce these these difficulties. Following Liu et al. [5], TMDs can be accessed in lepton-jet azimuthal correlation measurements, which are the same in the lepton-nucleon CM frame as they are in the laboratory frame. Lui et al. considered NC DIS, but the formalism can be extended to CC DIS as well. The advantage of this approach is that measuring the azimuthal angle for TMD studies only requires the neutrino's transverse momentum in the lab frame, which is in general better measured than the 3-momentum.

The jet-based measurements of Sivers asymmetries have the additional advantage of decoupling initial- and final-state TMD effects (at leading power in the jet radius). That is, they do not involve a convolution of TMD PDFs and fragmentation functions which can introduce strong correlations in global fits of SIDIS data [28, 29].

In this paper, we present the first calculations of neutrino-jet transverse single-spin asymmetries in CC DIS. We also perform feasibility studies of these channels using fast detector simulations and quantify the expected kinematic reach and statistical uncertainties.

The remainder of this paper is organized as follows. We describe the proposed measurements in Sec. II. In Sec. III, we present the theoretical framework. In Sec. IV we describe the fast detector simulation. Section V details the studies on the resolution of the kinematic reconstruction. We discuss event selection cuts to reduce NC DIS and photoproduction background in Sec. VI. The expected statistical precision of the proposed asymmetry measurements, as well as the results of the numerical calculations for the asymmetries, are given in Sec. VII. We conclude in Sec. VIII.

II. PROPOSED MEASUREMENTS

Following Liu et al. [5], we propose the measurement of the distribution of the azimuthal separation between the outgoing neutrino (as determined from the missing transverse momentum), and the jet. Due to the conservation of momentum, the jet and the neutrino are expected to be mostly back-to-back with one another. Therefore this distribution is expected to be centered at $\phi_{\rm jet} - \phi_\nu - \pi = 0$, with some width due to out-of-cone QCD radiation and the non-zero initial momentum of the struck quark.

We also propose to measure the transverse single-spin asymmetry in neutrino-jet correlations, also known as the left-right asymmetry

$$A_{\rm UT} = \frac{d\sigma^+ - d\sigma^-}{d\sigma^+ + d\sigma^-}\,. \tag{1}$$

Here, $d\sigma^\pm$ refers to the differential cross section measured with positive or negative transverse polarization of the proton. This is expected to modulate with respect to angular separation between the incoming proton spin, ϕ_S, and the momentum imbalance, ϕ_q, i.e.,

$$A_{\rm UT} = A_{\rm UT}^{\sin(\phi_S - \phi_q)} \sin(\phi_S - \phi_q). \tag{2}$$

Here, the momentum imbalance between the jet and the neutrino is defined by $\vec{q}_T = \vec{p}_T^{\,\rm jet} + \vec{p}_T^{\,\nu}$. This observable asymmetry is sensitive to the Sivers function [5, 8].

III. THEORETICAL FRAMEWORK

We follow the theoretical framework developed in Ref. [5, 7–9] for NC DIS. At the parton level, we consider the leading-order process $eq \to \nu q'$. The cross section is differential in the Bjorken x and the transverse momentum of the produced neutrino, p_T^ν, which is defined relative to the beam direction in the laboratory frame. The leading-order cross section can be written as

$$\frac{{\rm d}\sigma}{{\rm d}x\,{\rm d}^2\vec{p}_T^{\,\nu}} = \sum_q \sigma_0^{eq\to\nu q'} e_q^2\, f_q(x, \vec{b}_T, \mu)\,. \tag{3}$$

where the scale is chosen at the order of the hard scale of the process $\mu \sim p_T^\nu$. The prefactor σ_0 for initial quarks u and $\bar{d}$ are given by

$$\begin{aligned}\sigma_0^{eu\to\nu d} &= \frac{|\overline{\mathcal{M}}_{eu\to\nu d}|^2}{16\pi^2\hat{s}^2}\frac{\hat{t}}{x(\hat{t}-\hat{u})} \\ &= 8(G_F m_W^2)^2|V_{ud}|^2\frac{\hat{s}^2}{(\hat{t}-m_W^2)^2+m_W^2\Gamma_W^2}\frac{\hat{t}}{x(\hat{t}-\hat{u})} \end{aligned} \tag{4}$$

$$\begin{aligned}\sigma_0^{e\bar{d}\to\nu\bar{u}} &= \frac{|\overline{\mathcal{M}}_{e\bar{d}\to\nu\bar{u}}|^2}{16\pi^2\hat{s}^2}\frac{\hat{t}}{x(\hat{t}-\hat{u})} \\ &= 8(G_F m_W^2)^2|V_{ud}|^2\frac{\hat{u}^2}{(\hat{t}-m_W^2)^2+m_W^2\Gamma_W^2}\frac{\hat{t}}{x(\hat{t}-\hat{u})}\,, \end{aligned} \tag{5}$$

where $\hat{t}/(x(\hat{t}-\hat{u}))$ is the Jacobian from differential on neutrino rapidity y_ν to the Bjorken x variable and these

two variables are related by

$$x = \frac{p_T^\nu e^{y_\nu}}{\sqrt{s} - p_T^\nu e^{-y_\nu}}. \tag{6}$$

And the partonic Mandelstam variables in Eq. (4) and (5) can be written in terms of the kinematical variables of the produced neutrino and the center-of-mass energy, namely

$$\hat{s} = xs \tag{7}$$

$$\hat{t} = -Q^2 = -\sqrt{s}p_T^\nu e^{y_\nu} = -x\sqrt{s}p_T^{\rm jet} e^{-y_{\rm jet}}, \tag{8}$$

$$\hat{u} = -x\sqrt{s}p_T^\nu e^{-y_\nu} = -\sqrt{s}p_T^{\rm jet} e^{y_{\rm jet}} \tag{9}$$

where $p_T^{\rm jet}$ and $y_{\rm jet}$ denote the jet transverse momentum and rapidity, respectively.

A. Inclusive jet production

In this subsection, we derive the ν+jet production for vector-boson production (W^-) in polarized electron-proton scattering

$$p(P_A, \lambda_p, \vec{S}_T) + e(P_B, \lambda_e) \to {\rm jet}(P_J) + \nu(P_D) + X \tag{10}$$

To access TMD dynamics we study back-to-back neutrino-jet production in the ep collision frame,

$$P_A^\mu = P^+ n_+^\mu + \frac{M^2}{2P^+} n_-^\mu \approx P^+ n_+^\mu \,, \tag{11}$$

$$P_J^\mu = P_J^- n_-^\mu + \vec{P}_{JT} \,, \tag{12}$$

The differential cross section is given by

$$\begin{aligned}\frac{d\sigma^{ep\to\nu{\rm jet}X}}{dx d^2\vec{p}_T^\nu d^2 q_T} &= F_{UU} + \lambda_p F_{UL} \\ &+ |S_T| \Big[\sin(\phi_q - \phi_{S_A}) F_{UT}^{\sin(\phi_q - \phi_{S_A})} \\ &\quad + \cos(\phi_q - \phi_{S_A}) F_{UT}^{\cos(\phi_q - \phi_{S_A})} \Big] \\ &+ \lambda_e \Big[F_{LU} + \lambda_p F_{LL} \\ &\quad + |S_T| \sin(\phi_q - \phi_{S_A}) F_{LT}^{\sin(\phi_q - \phi_{S_A})} \\ &\quad + |S_T| \cos(\phi_q - \phi_{S_A}) F_{LT}^{\cos(\phi_q - \phi_{S_A})} \Big], \end{aligned} \tag{13}$$

where for the unpolarized case F_{UU}, in the limit of small imbalance $|\vec{q}_T| \ll p_T^{\rm jet} \sim p_T^\nu$, one has the TMD factorization of the differential cross section for unpolarized ep collision given by

$$\begin{aligned} F_{UU} = &\sum \frac{|\overline{\mathcal{M}}_{eq\to\nu q'}|^2}{16\pi^2 \hat{s}^2} H(Q,\mu) \mathcal{J}_q(p_T^{\rm jet} R, \mu) \\ &\times \int \frac{b_T db_T}{2\pi} J_0(q_T b_T) f_1^{\rm TMD}(x, b_T, \mu) \\ &\times S_q(b_T, y_{\rm jet}, R, \mu) \,, \end{aligned} \tag{14}$$

where $H(Q,\mu)$ is the hard function and takes into account virtual corrections at the scale Q. The jet function $\mathcal{J}_q$ is associated with collinear dynamics of the jet with natural scale $p_T^{\rm jet} R$ [30]. For our numerical results presented below we use the anti-k_T algorithm [31] and jet radius parameter $R = 1$. The quark TMD PDF including the appropriate soft factor denoted by $f_1^{\rm TMD}$ in b_T-space is defined by [9]

$$\begin{aligned} f_q^{(n),{\rm TMD}}(x, b_T, \mu) = &\frac{2\pi n!}{(M^2)^n} \int dk_T \, k_T \left(\frac{k_T}{b}\right)^n \\ &\times J_n(k_T b) \, \tilde{f}_q^{\rm TMD}\big(x, k_T^2, \mu\big) \,, \end{aligned} \tag{15}$$

where $n = 0$ by default. The remaining soft function S_q in Eq. (14) includes a contribution from the global soft function which depends on Wilson lines in the beam and jet directions, and the collinear-soft function associated with the soft jet dynamics. [Polarized case:] And other structure functions correlated with polarized electron or proton are defined in App. A. Specifically, for incoming electron with helicity λ_e, one substitutes $\sigma_0^{eq\to\nu q'}$ with $\sigma_0^{e_L q\to\nu q'}$ as given in Eq. (A6) and for polarized initial proton, take unpolarized quark in transversely polarized proton as an example,

$$\begin{aligned} F_{UT}^{\sin(\phi_q - \phi_{S_A})} = &\sum_q \frac{|\overline{\mathcal{M}}_{eq\to\nu q'}|^2}{16\pi^2 \hat{s}^2} H(Q,\mu) \mathcal{J}_q(p_T^{\rm jet} R, \mu) \\ &\times \int \frac{b_T^2 db_T}{4\pi M} J_1(q_T b_T) f_{1T}^{\perp(1),{\rm TMD}}(x, b_T, \mu) \\ &\times S_q(b_T, y_{\rm jet}, R, \mu) \,, \end{aligned} \tag{16}$$

where the structure function is related to the Sivers function $f_{1T}^{\perp(1),{\rm TMD}}(x, b_T, \mu)$ in b_T-space as defined in Eq. (15).

B. Hadron distribution inside jet

In this subsection, we study the hadron distribution in jet for vector-boson production (W^-) in polarized electron-proton scattering

$$\begin{aligned} &p(P_A, \lambda_p, \vec{S}_T) + e(P_B, \lambda_e) \\ &\qquad \to \big({\rm jet}(P_C) h(z_h, \vec{j}_\perp)\big) + \nu(P_D) + X \end{aligned} \tag{17}$$

In ep collision frame,

$$P_A^\mu = P^+ n_+^\mu + \frac{M^2}{2P^+} n_-^\mu \approx P^+ n_+^\mu \,, \tag{18}$$

$$P_C^\mu = P_h^- n_-^\mu + \frac{M_h^2}{2P_h^-} n_+^\mu \approx P_h^- n_-^\mu \,, \tag{19}$$

For unpolarized final-hadron state, one has TMD jet-fragmentation functions (JFFs) $\mathcal{D}_1$, $\mathcal{H}_1^\perp$ at leading-twist:

$$\Delta(z_h, \vec{j}_\perp) = \mathcal{D}_1^{h/q}(z_h, \vec{j}_\perp^2) \frac{\not{n}_-}{2} + i\mathcal{H}_1^{\perp,h/q}(z_h, \vec{j}_\perp^2) \frac{\not{j}_\perp}{z_h M_h} \frac{\not{n}_-}{2} \,. \tag{20}$$

Then we obtain

$$\begin{aligned} \frac{d\sigma^{ep\to\nu+\mathrm{jet}X}}{dx d^2\vec{p}_T^\nu d^2 q_T dz_h d^2 j_\perp} &= F_{UU}^h + \lambda_p F_{UL}^h \\ &+ |S_T| \Big[\cos(\phi_q - \phi_{S_A}) F_{UT}^{h,\cos(\phi_q-\phi_{S_A})} \\ &\quad + \sin(\phi_q - \phi_{S_A}) F_{UT}^{h,\sin(\phi_q-\phi_{S_A})} \Big] \\ &+ \lambda_e \Big[F_{LU}^h + \sin(\phi_q - \phi_{S_A}) F_{LT}^{h,\sin(\phi_q-\phi_{S_A})} \\ &\quad + \lambda_p F_{LL}^h + |S_T| \cos(\phi_q - \phi_{S_A}) F_{LT}^{\cos(\phi_q-\phi_{S_A})}) \Big] \,. \end{aligned} \tag{21}$$

with in total 8 terms[1] and the full expression and structure functions are provided in App. B. Following Refs. [30, 32–40], we can write the TMD factorization for the unpolarized cross section where, in addition, a hadron inside the jet is measured as:

$$\begin{aligned} &\frac{\mathrm{d}\sigma}{\mathrm{d}x\, \mathrm{d}^2\vec{p}_T^\nu\, \mathrm{d}^2\vec{q}_T\, \mathrm{d}z_h\, \mathrm{d}^2\vec{j}_T^h} = \\ &\times H(Q,\mu) \sum_q \sigma_0^{eq\to\nu q'}\, \mathcal{G}_q(z_h, \vec{j}_T, p_T^{\mathrm{jet}} R, \mu) \\ &\times \int \frac{\mathrm{d}^2\vec{b}_T}{(2\pi)^2} e^{i\vec{q}_T\cdot\vec{b}_T}\, f_1^{\mathrm{TMD}}(x, b_T, \mu)\, S_q(\vec{b}_T, y_{\mathrm{jet}}, R, \mu) \,. \end{aligned} \tag{22}$$

where z_h and j_T are respectively the longitudinal momentum fraction of the hadron inside the jet $z_h = \vec{p}_h \cdot \vec{p}_{\mathrm{jet}}/|\vec{p}_{\mathrm{jet}}|^2$ and the transverse momentum $\vec{j}_T^h = \vec{p}_h \times \vec{p}_{\mathrm{jet}}/|\vec{p}_{\mathrm{jet}}|^2$ of the hadron relative to the (standard) jet axis. In the factorized cross section, $\mathcal{G}_q^h$ is a TMD fragmenting jet function. It describes the hadron-in-jet measurement and replaces the jet function J_q in Eq. (13). At next-to-leading logarithmic (NLL) accuracy, we can write $\mathcal{G}_q^h$ as

$$\mathcal{G}_q^h(z_h, \vec{j}_T, p_T^{\mathrm{jet}} R) = \int \frac{\mathrm{d}^2\vec{b}_T'}{(2\pi)^2} e^{i\vec{j}_T\cdot\vec{b}_T'/z_h} D_q^h(z_h, \vec{b}_T', p_T^{\mathrm{jet}} R) \,. \tag{23}$$

Here we work in Fourier transform space and D_q^h is a TMD fragmentation function evaluated at the jet scale. We use the Fourier variable $\vec{b}_T'$ here to indicate that there is no convolution of the TMD fragmentation function with the TMD PDF in Eq. (22). See [39] for more details.

IV. SIMULATION

A. Event-Generation through Pythia8

We used Pythia8 [41] to simulate CC DIS events in unpolarized electron-proton and positron-proton collisions. We chose the energies of the lepton and proton as 10 GeV and 275 GeV, respectively. These beam-energy values, which yield a center-of-mass energy of $\sqrt{s} = 105$ GeV, correspond to the operation point that maximizes the luminosity of the EIC design [42]. Following Ref. [23], we selected events with $Q^2 > 100$ GeV^2. No QED radiative effects are included in the simulation to match the calculations in Sec. III [2].

We used the Fastjet3.3 package [44] to reconstruct jets with the anti-k_T algorithm [31] and jet radius parameter $R = 1$. The input particles for the generator-level jet finding are all stable particles ($c\tau > 10$ mm), except neutrinos.

Figure 2 shows our theoretical results with an uncertainty band for the ratio q_T/p_T^ν with the Pythia8 simulation for unpolarized ep collisions. The theoretical uncertainties are included by varying the scales μ and $p_T^{\mathrm{jet}} R$ by a factor of 2 around their central values and taking the envelope. A reasonable agreement between the theoretical curve and the Pythia8 results is observed. However,

[1] Note that all Collins-type jet fragmentation functions does not contribute in this process since chiral-odd functions must couple with other chiral-odd functions, then chirality between two $(1-\gamma_5)$ of the weak charged current vertex must be odd. As a result, one ends up with having $(1-\gamma_5)(1+\gamma_5) = 0$ for all chiral-odd function-related terms.

[2] Based on similar measurements in NC DIS [43], the QED corrections are expected to be small for the observables that we consider in this work, so not including them does not affect our conclusions.

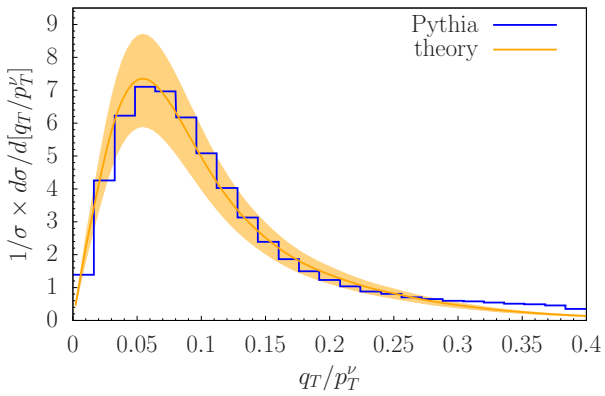

Figure 2. Normalized distribution of the ratio q_T/p_T^ν in unpolarized electron-proton collisions.

the tail of the q_T/p_T^ν distribution drops off slower at high q_T/p_T^ν in the PYTHIA8 simulations than in the theory curve. This can be attributed to multi-jet events, which are not included in the theory curve, at large q_T.

Fig. 3, shows a comparison of our theoretical results with the scale uncertainty (we vary the scales μ and $p_T^{\rm jet}R$ by a factor of 2 around their central values and fill between the curves) for j_T and z_h to the PYTHIA8 results for these variables using the simulated event sample described above, showing a reasonable agreement between the two.

In Fig. 4, we show the neutrino yields expected for 100 fb^{-1}, which can be collected in about a year of running at 10^{34} cm^{-2}s^{-1}, as a function of the neutrino's transverse momentum. We also show the mean of the parton momentum fraction x as a function of transverse momentum (red dots). Values up to $x = 0.8$ can be probed with jet/neutrino transverse momenta of $p_T = 45$ GeV, which corresponds to the kinematic limit. With 100 fb^{-1}, the statistical uncertainty on the differential cross-section measurement is expected to be negligible over the entire kinematic range. However, a high luminosity is needed to measure the corresponding spin asymmetry, as will be further detailed in Sec. VII.

B. Detector-response simulations

We used the DELPHES package [45] to perform fast detector simulation with parameters specified in Ref. [46]. The detector geometry we consider is a general-purpose detector including tracking, electromagnetic and hadronic calorimeters with coverage up to $|\eta| = 4.0$ and full azimuthal coverage, as described in the EIC yellow report [2]. This is in line with proposed EIC detector designs [47–49] that considered a high degree of hermeticity, which can be ensured with dedicated detectors at forward angles [50]. We show a representative charged-current event in Fig. 5.

To reconstruct jets in the detector-response simulation, we again used the FASTJET3.3 package [44] with the anti-k_T algorithm [31] and $R = 1$ [51]. The input for the jet algorithm was the set of particle-flow objects reconstructed with DELPHES.

In Fig. 6, we show the hadron-in-jet momenta for reconstructed $\pi^\pm$, as well as the average z_h in each bin in momentum. We find that the charged pions in jets can be found in the rapidity range from -0.5 to 3.5, and with momenta up to about 45 GeV, which can be identified with high purity with gas-based Cherenkov detectors [2].

V. EVENT RECONSTRUCTION AND KINEMATIC RESOLUTIONS

As typically done in colliders, neutrinos can be identified by measuring the missing transverse momentum, $\vec{p_T^{\rm miss}}$, which is defined as the vector sum of the transverse momenta of all measured particles (identified by the particle-flow algorithm to avoid double-counting). At the generator level all stable particles are included and it can be compared to the produced neutrino. The DELPHES fast smearing was shown to reproduce reasonably well the performance obtained from a comprehensive detector simulation of the CMS experiment over the entire range of $20 < |p_T^{\rm miss}| < 150$ GeV [45].

We define ϕ_ν as the azimuthal angle of $-\vec{p_T^{\rm miss}}$. We show the reconstruction performance of ϕ_ν in Fig. 7. The standard deviation is less than 0.06 radians, which is of similar order to the di-jet azimuthal-angle resolution of the measurement presented in Ref. [52].

We employ the Jacquet-Blondel (JB) method of Ref. [53] to reconstruct the lepton kinematics. The event inelasticity is given by $y_{JB} = \sum(E_i - p_{z,i})/(2E_e)$ where the sum is over all the reconstructed particles. The four-momentum transfer is given by $Q^2_{JB} = (p_T^{\rm miss})^2/(1-y_{JB})$ and the Björken scaling variable is $x_{JB} = Q^2_{JB}/(sy_{JB})$, where $s = 4E_eE_p$ and E_e (E_p) is the energy of the electron (proton) beam. The resolution of reconstructing these variables was investigated in Ref. [23], and found to be reasonable for all three of these variables. The performance of the Jacquet-Blondel method might be improved with machine-learning methods such as those proposed in Refs. [54, 55].

Figure 8, we compare the reconstructed values of q_T/p_T^ν

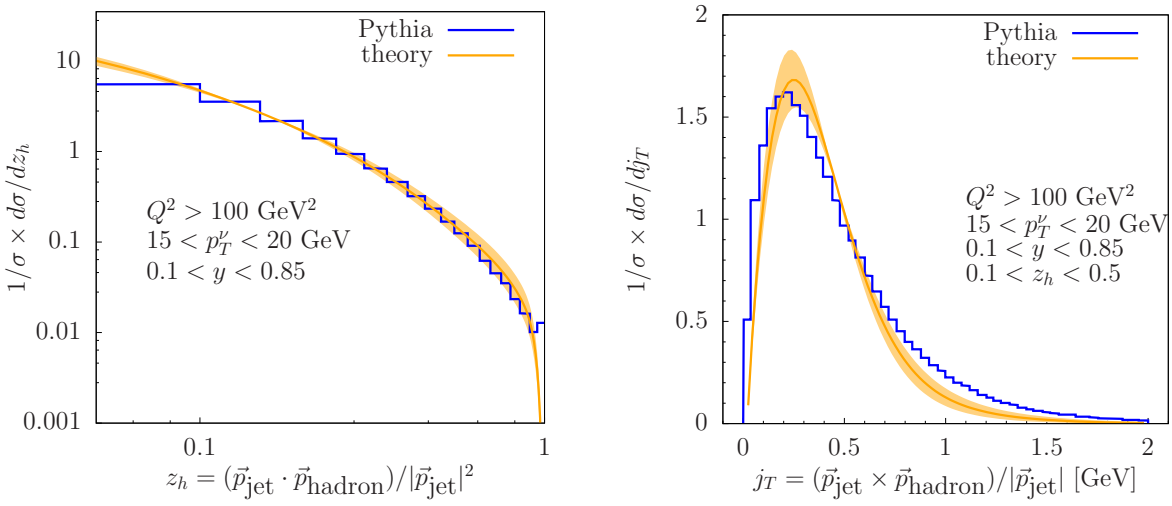

Figure 3. Distributions of the hadron-in-jet longitudinal-momentum fraction z_h (left) and the transverse-momentum j_T (right) of e^-p events generated in PYTHIA 8 [41] (blue) compared to our theoretical results with scale uncertainties (orange).

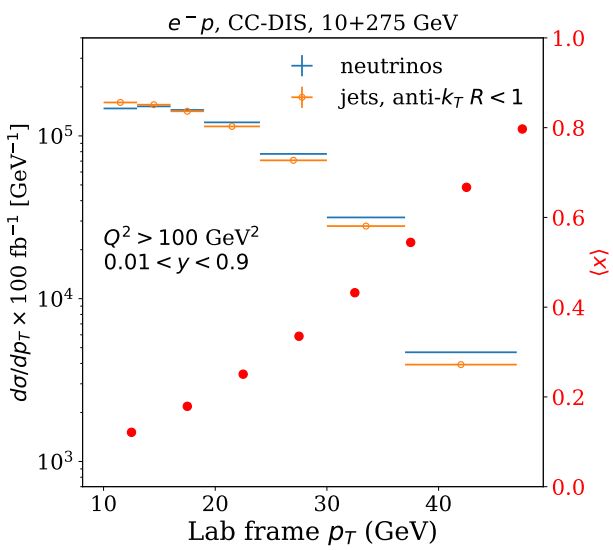

Figure 4. Expected yield of neutrinos and jets in CC DIS with an electron beam and 100 fb^{-1} integrated luminosity. In addition, we show the average x which is probed as a function of the neutrino transverse momentum in the laboratory frame. The cross-sections generated in PYTHIA have been scaled to match the total cross-sections calculated at NLO in Ref. [23].

with the value obtained at generator level. In the bottom panel of this figure, we show that the the "bin purity", or fraction of events generated in a given bin that are reconstructed to be in the same bin, is more than 50%

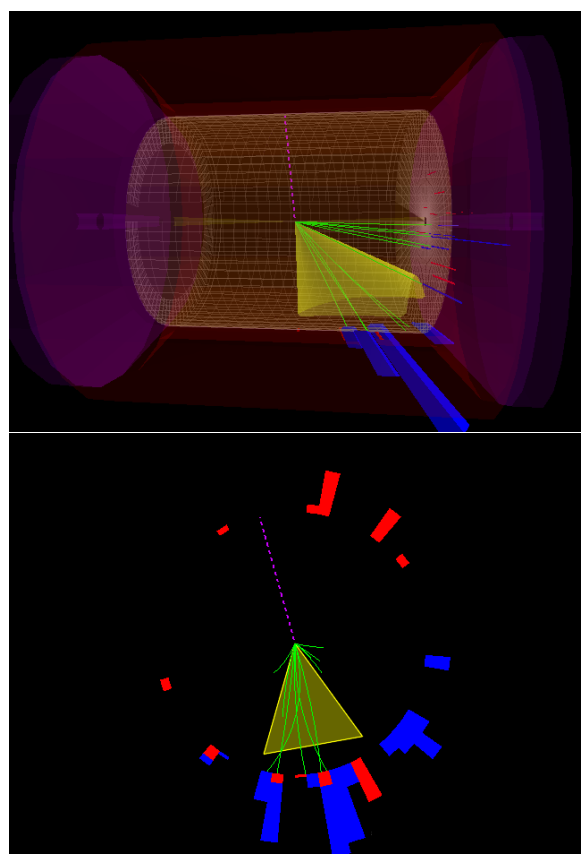

Figure 5. Display of simulated CC DIS event using DELPHES [45]. Top: 3D view. Bottom: Transverse view.

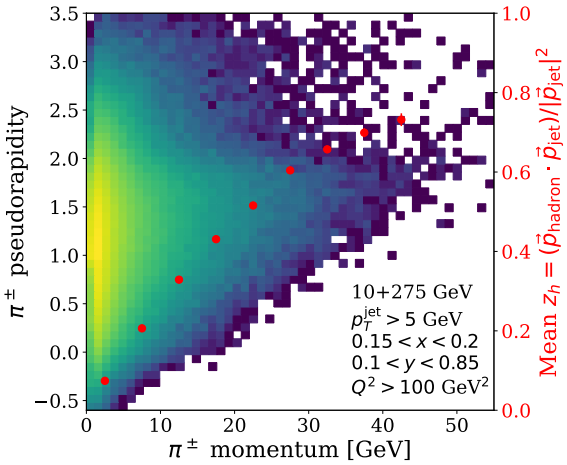

Figure 6. Pseudorapidity and momentum distribution for charged pions in jets with $p_T > 5$ GeV in e^-p CC DIS. The average longitudinal-momentum fraction of the hadron with respect to the jet axis is shown by the red dots.

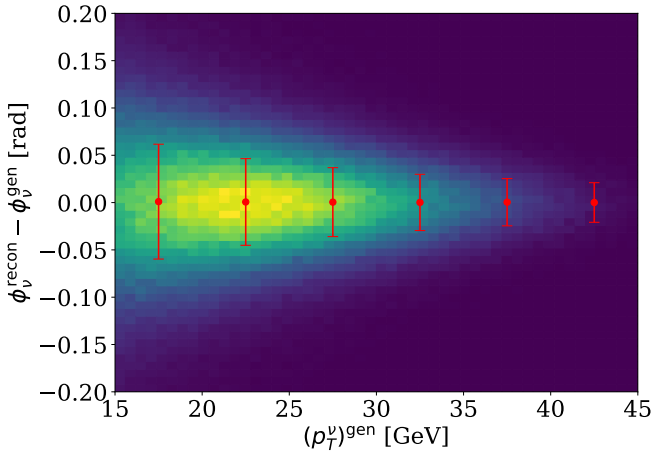

Figure 7. Performance of the reconstruction of ϕ_ν in CC DIS events. Red error bars indicate the mean and standard deviations within slices of p_T^ν

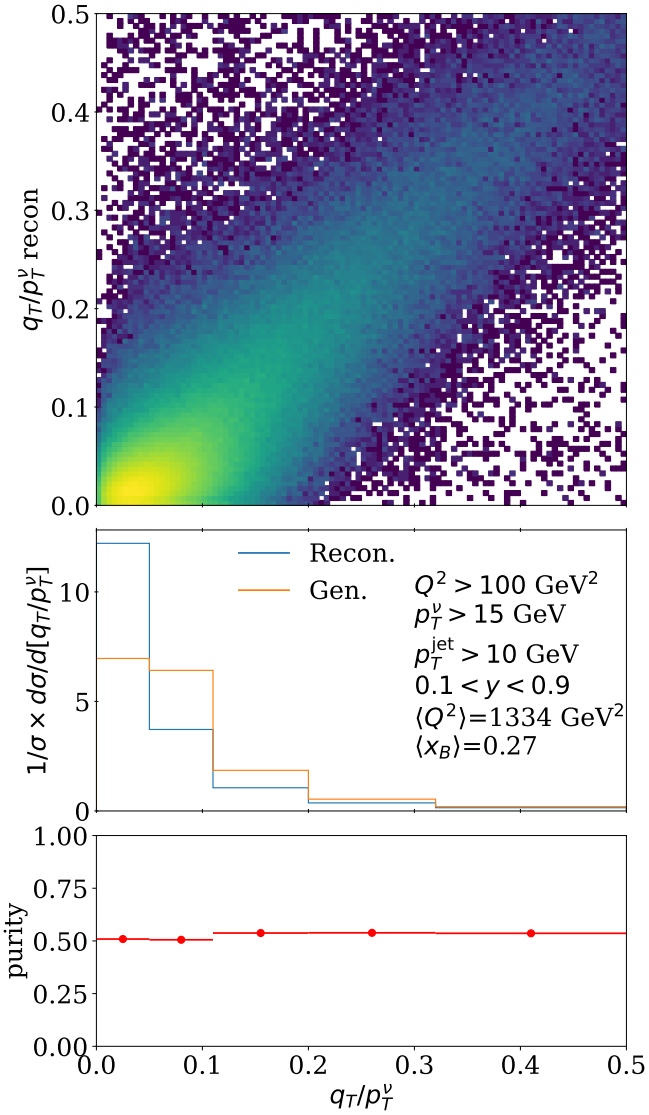

Figure 8. Top: 2D histogram of the generated q_T/p_T^ν (x axis) vs. the reconstructed value (y axis). Middle: Spectra of reconstructed and generated q_T/p_T^ν, using five bins. Bottom: Purity as a function of q_T/p_T^ν.

for a particular binning scheme. Such level of purity is amenable to standard unfolding methods.

VI. SUPPRESSION OF NC DIS AND PHOTOPRODUCTION BACKGROUNDS

Given the relatively low rate of charged-current DIS events relative to neutral-current DIS and photoproduction, the background suppression generally represents a significant challenge. If the scattered electron is missed, the event topologies of neutral- and charged-current DIS are identical. We expect that this scenario will be significantly suppressed at the EIC compared to the HERA experiments thanks to improved low-angle taggers for low Q^2 events [2], although the performance of such systems is hard to estimate at this point.

Rather than to use a low-angle scattering veto to sup-

press photoproduction, we follow the approach used by the CC DIS analyses at HERA [13] that relied on two kinematic variables: $\delta = \sum_i E_i - p_{z,i}$ (where E_i and $p_{z,i}$ are the reconstructed energy and longitudinal momentum of detected particles, and the sum runs over all reconstructed particles) and the ratio of the anti-parallel component, V_{AP}, to the parallel component, V_P, of the hadronic state. These are defined as

$$V_{AP} = -\sum_i \vec{p}_{T,i} \cdot \hat{n}, \quad \text{for } \vec{p}_{T,i} \cdot \hat{n} < 0 \tag{24}$$

and

$$V_P = \sum_i \vec{p}_{T,i} \cdot \hat{n}, \quad \text{for } \vec{p}_{T,i} \cdot \hat{n} > 0 \tag{25}$$

where $\vec{p}_{T,i}$ are the transverse parts of the individual particles' momenta, $\hat{n} = -\vec{p}_T^{\,\nu}/|\vec{p}_T^{\,\nu}|$, and the sums are over all reconstructed particles in the event. The purpose on the cuts on this variable was to ensure an azimuthally collimated energy flow. For charged-current events, the ratio V_{AP}/V_P is small, in particular for the events that we are interested in that are suitable for TMD studies.

To test the efficacy of these variables for background reduction, we ran simulations of NC DIS and photoproduction reactions in the same manner as our CC DIS simulations (see Sec. IV). We chose to use the following cuts $p_T^\nu > 15$ GeV, $V_{AP}/V_P < 0.35$, and $\delta < 30$ GeV (which are similar to those used in Ref. [13]). We found that ≈30% of the generated CC DIS events passed these cuts, whereas only 0.0005±0.0002% of photoproduction events passed these cuts. None of the 1.5 million NC DIS events passed these cuts. However, the photoproduction has a cross section that is three orders of magnitude larger than that of CC DIS (58 nb, compared to 14 pb, as estimated in Pythia). Therefore, we estimate that about 8±3% of the event sample would be background from photoproduction, when only using kinematic variables and no low-angle electron tagger.

VII. STATISTICAL PRECISION OF ASYMMETRY MEASUREMENTS

We show in Fig. 9 the statistical uncertainty projected for the transverse single-spin asymmetry, $A_{UT}^{\sin(\phi_q - \phi_{S_A})}$, assuming a luminosity of 100 fb^{-1}. The absolute uncertainty of the asymmetry measurement is estimated to be $\sqrt{2}/(p\sqrt{N})$, where p is the polarization of the proton beam, 70%, and N is the number of events in a given bin that pass our cuts, scaled to match the NLO total inclusive cross sections of Ref. [23] and an integrated luminosity of 100 fb^{-1}. Following Ref. [56], we include the factor of $\sqrt{2}$ factor to account for the fitting of the azimuthal modulations.

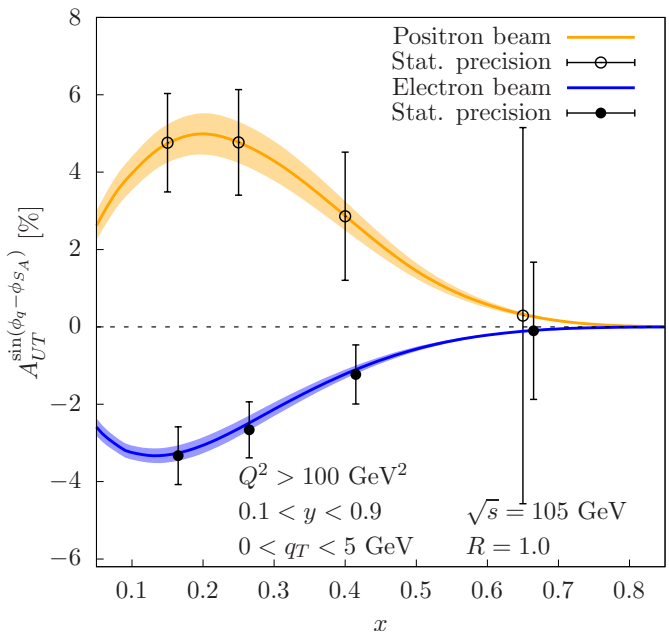

Figure 9. Projected statistical precision for the neutrino-jet asymmetry, which is sensitive to the Sivers distribution for positron-proton collision (open circles) and electron-proton collision (closed circles), for 100 fb^{-1}. The curves represent theoretical results and their uncertainty bands are obtained by the uncertainty of the extracted Sivers function in Ref. [57].

We compare these results to the numerical results of our calculations (see Sec. III), which are integrated over the transverse momentum imbalance $0 < q_T < 5$ GeV and inelasticity $0.1 < y < 0.9$. The uncertainty bands of the calculation curves were determined according to Ref. [57].

The projected statistical error bars are smaller than the predicted asymmetry for the first three bins, allowing the proposed measurement to provide a decent comparison with the model. For the highest bin in x, the statistical errors are much larger than the predicted asymmetry.

VIII. SUMMARY AND CONCLUSIONS

We have proposed a novel channel to study the 3D structure of the nucleon at the EIC that offers unique sensitive to quark flavor: charge-current deep-inelastic scattering.

We have presented first calculation of the azimuthal

correlation as well as transverse-spin asymmetries. These are much bigger than those corresponding for the electron-jet channel, which partially compensates the loss of statistical precision due to having lower expected rates than for neutral-current interactions.

We have used the expected EIC machine parameters of luminosity and energy to estimate the kinematic reach of this measurement. We showed that an excellent coverage of high-x region can be achieved. We have also used fast detector simulations to estimate the performance on neutrino (missing energy) reconstruction, as well as neutrino-jet momentum imbalance.

While much of the emphasis of the EIC project lies in the low-x and gluon studies, we show that charged-current deep-inelastic scattering represents an excellent way to probe the high-x region of the valence quarks up to $x = 0.8$. This channel will take full advantage of key aspects of the EIC: the high-luminosity, high beam polarization, as well as hermeticity of the EIC detectors. This represents an important channel that adds to the growing program that can be carried out with jets physics at the EIC.

ACKNOWLEDGEMENTS

This work was supported by MRPI program of the University of California Office of the President, award number 00010100. M.A. was supported through DOE Contract No. DE-AC05-06OR23177 under which JSA operates the Thomas Jefferson National Accelerator Facility. Z.K. is supported by the National Science Foundation under grant No. PHY-1945471. F.R. was supported by the Simons Foundation under the Simons Bridge program for Postdoctoral Fellowships at SCGP and YITP award number 815892; the NSF, award number 1915093; the DOE Contract No. DE-AC05-06OR23177, under which Jefferson Science Associates, LLC operates Jefferson Lab, and Old Dominion University.

[1] A. Accardi *et al.*, "Electron Ion Collider: The Next QCD Frontier," *Eur. Phys. J.* **A52** no. 9, (2016) 268, arXiv:1212.1701 [nucl-ex].

[2] R. Abdul Khalek *et al.*, "Science Requirements and Detector Concepts for the Electron-Ion Collider: EIC Yellow Report," *Nucl. Phys. A* **1026** (2022) 122447, arXiv:2103.05419 [physics.ins-det].

[3] D. Gutierrez-Reyes, I. Scimemi, W. J. Waalewijn, and L. Zoppi, "Transverse momentum dependent distributions with jets," *Phys. Rev. Lett.* **121** no. 16, (2018) 162001, arXiv:1807.07573 [hep-ph].

[4] D. Gutierrez-Reyes, I. Scimemi, W. J. Waalewijn, and L. Zoppi, "Transverse momentum dependent distributions in e^+e^- and semi-inclusive deep-inelastic scattering using jets," *JHEP* **10** (2019) 031, arXiv:1904.04259 [hep-ph].

[5] X. Liu, F. Ringer, W. Vogelsang, and F. Yuan, "Lepton-jet Correlations in Deep Inelastic Scattering at the Electron-Ion Collider," *Phys. Rev. Lett.* **122** no. 19, (2019) 192003, arXiv:1812.08077 [hep-ph].

[6] Z.-B. Kang, K. Lee, and F. Zhao, "Polarized jet fragmentation functions," *Physics Letters B* **809** (2020) 135756. https://www.sciencedirect.com/science/article/pii/S0370269320305591.

[7] M. Arratia, Z.-B. Kang, A. Prokudin, and F. Ringer, "Jet-based measurements of sivers and collins asymmetries at the future electron-ion collider," *Phys. Rev. D* **102** (Oct, 2020) 074015. https://link.aps.org/doi/10.1103/PhysRevD.102.074015.

[8] X. Liu, F. Ringer, W. Vogelsang, and F. Yuan, "Lepton-jet Correlation in Deep Inelastic Scattering," *Phys. Rev. D* **102** no. 9, (2020) 094022, arXiv:2007.12866 [hep-ph].

[9] Z.-B. Kang, K. Lee, D. Y. Shao, and F. Zhao, "Spin asymmetries in electron-jet production at the future electron ion collider," *JHEP* **11** (2021) 005, arXiv:2106.15624 [hep-ph].

[10] R. Abdul Khalek *et al.*, "Snowmass 2021 White Paper: Electron Ion Collider for High Energy Physics," in *2022 Snowmass Summer Study*. 3, 2022. arXiv:2203.13199 [hep-ph].

[11] K. Lee, J. Mulligan, M. Płoskoń, F. Ringer, and F. Yuan, "Machine learning-based jet and event classification at the Electron-Ion Collider with applications to hadron structure and spin physics," arXiv:2210.06450 [hep-ph].

[12] **H1** Collaboration, F. Aaron *et al.*, "Inclusive Deep Inelastic Scattering at High Q^2 with Longitudinally Polarised Lepton Beams at HERA," *JHEP* **09** (2012) 061, arXiv:1206.7007 [hep-ex].

[13] **ZEUS** Collaboration, H. Abramowicz *et al.*, "Measurement of high-Q^2 charged current deep inelastic scattering cross sections with a longitudinally polarised positron beam at HERA," *Eur. Phys. J. C* **70** (2010) 945–963, arXiv:1008.3493 [hep-ex].

[14] **ZEUS** Collaboration, S. Chekanov *et al.*, "Measurement of charged current deep inelastic scattering cross sections with a longitudinally polarised electron beam at HERA," *Eur. Phys. J. C* **61** (2009) 223–235, arXiv:0812.4620 [hep-ex].

[15] **ZEUS** Collaboration, S. Chekanov *et al.*, "Measurement of high Q^2 charged current cross-sections in e^-p deep inelastic scattering at HERA," *Phys. Lett. B* **539** (2002) 197–217, arXiv:hep-ex/0205091. [Erratum:

Phys.Lett.B 552, 308–308 (2003)].

[16] **ZEUS** Collaboration, J. Breitweg *et al.*, "Measurement of high Q**2 charged current e+ p deep inelastic scattering cross-sections at HERA," *Eur. Phys. J. C* **12** (2000) 411–428, arXiv:hep-ex/9907010. [Erratum: Eur.Phys.J.C 27, 305–309 (2003)].

[17] **ZEUS** Collaboration, M. Derrick *et al.*, "Study of charged current ep interactions at $Q^2 > 200 - Gev^2$ with the ZEUS detector at HERA," *Z. Phys. C* **72** (1996) 47–64, arXiv:hep-ex/9606014.

[18] **H1, ZEUS** Collaboration, H. Abramowicz *et al.*, "Combination of measurements of inclusive deep inelastic $e^{\pm}p$ scattering cross sections and QCD analysis of HERA data," *Eur. Phys. J. C* **75** no. 12, (2015) 580, arXiv:1506.06042 [hep-ex].

[19] **ZEUS** Collaboration, S. Chekanov *et al.*, "Jet production in charged current deep inelastic e+ p scattering at HERA," *Eur. Phys. J.* **C31** (2003) 149–164, arXiv:hep-ex/0306018 [hep-ex].

[20] **ZEUS** Collaboration, S. Chekanov *et al.*, "Multi-jet cross-sections in charged current e+- p scattering at HERA," *Phys. Rev.* **D78** (2008) 032004, arXiv:0802.3955 [hep-ex].

[21] T. Gehrmann, A. Huss, J. Niehues, A. Vogt, and D. M. Walker, "Jet production in charged-current deep-inelastic scattering to third order in QCD," *Phys. Lett.* **B792** (2019) 182–186, arXiv:1812.06104 [hep-ph].

[22] J. Blumlein, "The Theory of Deeply Inelastic Scattering," *Prog. Part. Nucl. Phys.* **69** (2013) 28–84, arXiv:1208.6087 [hep-ph].

[23] E. C. Aschenauer, T. Burton, T. Martini, H. Spiesberger, and M. Stratmann, "Prospects for Charged Current Deep-Inelastic Scattering off Polarized Nucleons at a Future Electron-Ion Collider," *Phys. Rev.* **D88** (2013) 114025, arXiv:1309.5327 [hep-ph].

[24] H. Avakian, B. Parsamyan, and A. Prokudin, "Spin orbit correlations and the structure of the nucleon," *Riv. Nuovo Cim.* **42** no. 1, (2019) 1–48, arXiv:1909.13664 [hep-ex].

[25] M. Anselmino, P. Gambino, and J. Kalinowski, "Polarized deep inelastic scattering at high-energies and parity violating structure functions," *Z. Phys. C* **64** (1994) 267–274, arXiv:hep-ph/9401264.

[26] K.-b. Chen and W.-h. Yang, "Parity violating semi-inclusive deeply inelastic scattering at the Electron-Ion Collider," arXiv:2004.01359 [hep-ph].

[27] W.-h. Yang, "Charged current semi-inclusive deeply inelastic scattering at the electron-ion collider," *Phys. Rev. D* **103** (Jan, 2021) 016011. https://link.aps.org/doi/10.1103/PhysRevD.103.016011.

[28] A. Bacchetta, F. Delcarro, C. Pisano, M. Radici, and A. Signori, "Extraction of partonic transverse momentum distributions from semi-inclusive deep-inelastic scattering, Drell-Yan and Z-boson production," *JHEP* **06** (2017) 081, arXiv:1703.10157 [hep-ph]. [Erratum: JHEP 06, 051 (2019)].

[29] I. Scimemi and A. Vladimirov, "Non-perturbative structure of semi-inclusive deep-inelastic and Drell-Yan scattering at small transverse momentum," *JHEP* **06** (2020) 137, arXiv:1912.06532 [hep-ph].

[30] S. D. Ellis, C. K. Vermilion, J. R. Walsh, A. Hornig, and C. Lee, "Jet Shapes and Jet Algorithms in SCET," *JHEP* **11** (2010) 101, arXiv:1001.0014 [hep-ph].

[31] M. Cacciari, G. P. Salam, and G. Soyez, "The anti-k_t jet clustering algorithm," *JHEP* **04** (2008) 063, arXiv:0802.1189 [hep-ph].

[32] F. Yuan, "Azimuthal asymmetric distribution of hadrons inside a jet at hadron collider," *Phys. Rev. Lett.* **100** (2008) 032003, arXiv:0709.3272 [hep-ph].

[33] M. Procura and I. W. Stewart, "Quark Fragmentation within an Identified Jet," *Phys. Rev. D* **81** (2010) 074009, arXiv:0911.4980 [hep-ph]. [Erratum: Phys.Rev.D 83, 039902 (2011)].

[34] A. Jain, M. Procura, and W. J. Waalewijn, "Parton Fragmentation within an Identified Jet at NNLL," *JHEP* **05** (2011) 035, arXiv:1101.4953 [hep-ph].

[35] T. Kaufmann, A. Mukherjee, and W. Vogelsang, "Hadron Fragmentation Inside Jets in Hadronic Collisions," *Phys. Rev. D* **92** no. 5, (2015) 054015, arXiv:1506.01415 [hep-ph]. [Erratum: Phys.Rev.D 101, 079901 (2020)].

[36] Z.-B. Kang, F. Ringer, and I. Vitev, "Jet substructure using semi-inclusive jet functions in SCET," *JHEP* **11** (2016) 155, arXiv:1606.07063 [hep-ph].

[37] R. Bain, Y. Makris, and T. Mehen, "Transverse Momentum Dependent Fragmenting Jet Functions with Applications to Quarkonium Production," *JHEP* **11** (2016) 144, arXiv:1610.06508 [hep-ph].

[38] Z.-B. Kang, X. Liu, F. Ringer, and H. Xing, "The transverse momentum distribution of hadrons within jets," *JHEP* **11** (2017) 068, arXiv:1705.08443 [hep-ph].

[39] Z.-B. Kang, A. Prokudin, F. Ringer, and F. Yuan, "Collins azimuthal asymmetries of hadron production inside jets," *Phys. Lett.* **B774** (2017) 635–642, arXiv:1707.00913 [hep-ph].

[40] Z.-B. Kang, K. Lee, J. Terry, and H. Xing, "Jet fragmentation functions for Z-tagged jets," *Phys. Lett. B* **798** (2019) 134978, arXiv:1906.07187 [hep-ph].

[41] T. Sjostrand, S. Mrenna, and P. Z. Skands, "A Brief Introduction to PYTHIA 8.1," *Comput. Phys. Commun.* **178** (2008) 852–867, arXiv:0710.3820 [hep-ph].

[42] BNL, "An electron-ion collider study." https://wiki.bnl.gov/eic/upload/EIC.Design.Study.pdf, 2020.

[43] **H1** Collaboration, V. Andreev *et al.*, "Measurement of Lepton-Jet Correlation in Deep-Inelastic Scattering with the H1 Detector Using Machine Learning for Unfolding," *Phys. Rev. Lett.* **128** no. 13, (2022) 132002, arXiv:2108.12376 [hep-ex].

[44] M. Cacciari, G. P. Salam, and G. Soyez, "FastJet User Manual," *Eur. Phys. J.* **C72** (2012) 1896, arXiv:1111.6097 [hep-ph].

[45] **DELPHES 3** Collaboration, J. de Favereau, C. Delaere, P. Demin, A. Giammanco, V. Lemaître, A. Mertens, and M. Selvaggi, "DELPHES 3, A modular framework for fast simulation of a generic collider experiment," *JHEP* **02** (2014) 057, arXiv:1307.6346 [hep-ex].

[46] M. Arratia and S. Sekula, "A Delphes card for the EIC yellow-report detector," arXiv:2103.06886 [physics.ins-det].

[47] J. K. Adkins *et al.*, "Design of the ECCE Detector for the Electron Ion Collider," arXiv:2209.02580 [physics.ins-det].

[48] **ATHENA** Collaboration, J. Adam *et al.*, "ATHENA detector proposal — a totally hermetic electron nucleus apparatus proposed for IP6 at the Electron-Ion Collider," *JINST* **17** no. 10, (2022) P10019, arXiv:2210.09048 [physics.ins-det].

[49] **CORE** Collaboration, R. Alarcon *et al.*, "CORE – a COmpact detectoR for the EIC," arXiv:2209.00496 [physics.ins-det].

[50] M. Arratia *et al.*, "A high-granularity calorimeter insert based on SiPM-on-tile technology at the future Electron-Ion Collider," arXiv:2208.05472 [physics.ins-det].

[51] P. Newman and M. Wing, "The Hadronic Final State at HERA," *Rev. Mod. Phys.* **86** no. 3, (2014) 1037, arXiv:1308.3368 [hep-ex].

[52] **STAR** Collaboration, B. I. Abelev *et al.*, "Measurement of transverse single-spin asymmetries for di-jet production in proton-proton collisions at s**(1/2) = 200-GeV," *Phys. Rev. Lett.* **99** (2007) 142003, arXiv:0705.4629 [hep-ex].

[53] U. Amaldi *et al.*, "REPORT FROM THE STUDY GROUP ON DETECTORS FOR CHARGED CURRENT EVENTS," in *ECFA Study of an ep Facility for Europe*. 1979.

[54] M. Arratia, D. Britzger, O. Long, and B. Nachman, "Reconstructing the kinematics of deep inelastic scattering with deep learning," *Nucl. Instrum. Meth. A* **1025** (2022) 166164, arXiv:2110.05505 [hep-ex].

[55] M. Arratia, D. Britzger, O. Long, and B. Nachman, "Optimizing observables with machine learning for better unfolding," *JINST* **17** no. 07, (2022) P07009, arXiv:2203.16722 [hep-ex].

[56] M. Anselmino *et al.*, "Transverse Momentum Dependent Parton Distribution/Fragmentation Functions at an Electron-Ion Collider," *Eur. Phys. J.* **A47** (2011) 35, arXiv:1101.4199 [hep-ex].

[57] M. G. Echevarria, Z.-B. Kang, and J. Terry, "Global analysis of the Sivers functions at NLO+NNLL in QCD," *JHEP* **01** (2021) 126, arXiv:2009.10710 [hep-ph].

[58] Z.-B. Kang, F. Ringer, and I. Vitev, "The semi-inclusive jet function in SCET and small radius resummation for inclusive jet production," *JHEP* **10** (2016) 125, arXiv:1606.06732 [hep-ph].

Appendix A: Inclusive jet production

In the process of $e+p\to\nu+\text{jet}+X$ where the incoming proton is unpolarized and the incoming electron can be unpolarized or have helicity λ_e, the squared matrix element is given by

$$
\begin{aligned}
|\mathcal{M}|^2 =& \left(\frac{e^2}{2\sin^2\theta_w}\right)^2 |V_{ud}|^2 \frac{(g^{\mu\nu}-\frac{q^\mu q^\nu}{m_W^2})(g^{\mu'\nu'}-\frac{q^{\mu'}q^{\nu'}}{m_W^2})}{(q^2-m_W^2)^2+(m_W\Gamma_W)^2} \\
&\times \mathrm{Tr}\left[\not{P}_D\gamma^\mu\left(\frac{1-\gamma_5}{2}\right)(\not{P}_B+\lambda_e\gamma_5\not{P}_B)\gamma^{\mu'}\left(\frac{1-\gamma_5}{2}\right)\right] \\
&\times \mathrm{Tr}\left[\hat{\not{P}}_C\gamma^\nu\left(\frac{1-\gamma_5}{2}\right)\hat{\not{P}}_A\gamma^{\nu'}\left(\frac{1-\gamma_5}{2}\right)\right] \\
=& 8(G_F m_W^2)^2|V_{ud}|^2\frac{1}{(\hat{t}-m_W^2)^2+(m_W\Gamma_W)^2} \\
&\times \mathrm{Tr}\left[\not{P}_D\gamma^\mu\left(\frac{1-\gamma_5}{2}\right)(\not{P}_B+\lambda_e\gamma_5\not{P}_B)\gamma^{\nu}\left(\frac{1-\gamma_5}{2}\right)\right] \\
&\times \mathrm{Tr}\left[\hat{\not{P}}_C\gamma_\mu\left(\frac{1-\gamma_5}{2}\right)\hat{\not{P}}_A\gamma_{\nu}\left(\frac{1-\gamma_5}{2}\right)\right], \qquad \text{(A1)}
\end{aligned}
$$

where $\hat{P}_A = xP_A$ and $\hat{P}_C = P_J$ and we have applied $\frac{4G_F}{\sqrt{2}} = \frac{e^2}{2m_W^2\sin^2\theta_w}$. For a longitudinally polarized proton with helicity λ_p, one simply substitute $\hat{\not{P}}_A \to \gamma_5\hat{\not{P}}_A$. For a transversely polarized proton with transverse spin S_T^i, $\hat{\not{P}}_A \to \gamma_5\gamma_i\hat{\not{P}}_A$ (though the trace of hadronic tensor is always 0 for transversely polarized proton). The leptonic tensor is given by electron and left-handed neutrino:

$$
\begin{aligned}
L^{\mu\nu} &= \mathrm{Tr}\left[\not{P}_D\gamma^\mu(1+\lambda_e\gamma_5)\not{P}_B\gamma^\nu\left(\frac{1-\gamma_5}{2}\right)\right] \\
&= (1-\lambda_e)\left(P_B^\mu P_D^\nu + P_B^\nu P_D^\mu - g^{\mu\nu}P_B\cdot P_D + i\epsilon^{\mu\nu P_B P_D}\right) \\
&= L_u^{\mu\nu} + L_p^{\mu\nu}, \qquad \text{(A2)}
\end{aligned}
$$

where

$$
L_u^{\mu\nu} = \left(P_B^\mu P_D^\nu + P_B^\nu P_D^\mu - g^{\mu\nu}P_B\cdot P_D + i\epsilon^{\mu\nu P_B P_D}\right), \qquad \text{(A3)}
$$

$$
L_p^{\mu\nu} = -\lambda_e\left(P_B^\mu P_D^\nu + P_B^\nu P_D^\mu - g^{\mu\nu}P_B\cdot P_D + i\epsilon^{\mu\nu P_B P_D}\right), \qquad \text{(A4)}
$$

represent the polarized and unpolarized components of the leptonic tensor.

Then one obtains the differential cross section given by

Eq. (13) with structure functions defined by

$$
\begin{aligned}
F_{UU} =& \sum \frac{|\overline{\mathcal{M}}_{eq\to\nu q'}|^2}{16\pi^2\hat{s}^2} H(Q,\mu)\mathcal{J}_q(p_T^{\rm jet}R,\mu) \\
&\times \int \frac{b_T db_T}{2\pi} J_0(q_T b_T) f_1^{\rm TMD}(x,b_T,\mu) \\
&\times S_q(b_T, y_{\rm jet}, R, \mu)\,, \\
=& \mathcal{C}\left[f_1\right]_{eq\to\nu q'}\,, \qquad \text{(A5)} \\
F_{LU} =& \mathcal{C}\left[f_1\right]_{e_L q\to\nu q'}\,, \qquad \text{(A6)} \\
F_{UL} =& \mathcal{C}\left[g_{1L}\right]_{eq_L\to\nu q'}\,, \qquad \text{(A7)} \\
F_{LL} =& \mathcal{C}\left[g_{1L}\right]_{e_L q_L\to\nu q'}\,, \qquad \text{(A8)}
\end{aligned}
$$

$$
\begin{aligned}
F_{UT}^{\cos(\phi_q-\phi_{S_A})} =& \sum \frac{|\overline{\mathcal{M}}_{eq_L\to\nu q'}|^2}{16\pi^2\hat{s}^2} H(Q,\mu)\mathcal{J}_q(p_T^{\rm jet}R,\mu) \\
&\times \int \frac{b_T^2 db_T}{4\pi M} J_1(q_T b_T) g_{1T}^{(1),\rm TMD}(x,b_T,\mu) \\
&\times S_q(b_T, y_{\rm jet}, R, \mu)\,, \\
=& \tilde{\mathcal{C}}\left[g_{1T}\right]_{eq_L\to\nu q'}\,, \qquad \text{(A9)} \\
F_{LT}^{\cos(\phi_q-\phi_{S_A})} =& \tilde{\mathcal{C}}\left[g_{1T}\right]_{e_L q_L\to\nu q'}\,, \qquad \text{(A10)} \\
F_{UT}^{\sin(\phi_q-\phi_{S_A})} =& \tilde{\mathcal{C}}\left[f_{1T}^{\perp}\right]_{eq\to\nu q'}\,, \qquad \text{(A11)} \\
F_{LT}^{\sin(\phi_q-\phi_{S_A})} =& \tilde{\mathcal{C}}\left[f_{1T}^{\perp}\right]_{e_L q\to\nu q'}\,, \qquad \text{(A12)}
\end{aligned}
$$

where the semi-inclusive jet function $\mathcal{J}_q(p_T^{\rm jet}R,\mu)$ are introduced in [58]. The relevant leading-order matrix elements squared are given by

$$
|\overline{\mathcal{M}}_{eu\to\nu d}|^2 = 8(G_F m_W^2)^2 |V_{ud}|^2 \frac{\hat{s}^2}{(\hat{t}-m_W^2)^2 + m_W^2\Gamma_W^2}\,, \qquad \text{(A13)}
$$

$$
|\overline{\mathcal{M}}_{e\bar{d}\to\nu\bar{u}}|^2 = 8(G_F m_W^2)^2 |V_{ud}|^2 \frac{\hat{u}^2}{(\hat{t}-m_W^2)^2 + m_W^2\Gamma_W^2}\,, \qquad \text{(A14)}
$$

$$
\begin{aligned}
|\overline{\mathcal{M}}_{e_L q\to\nu q'}|^2 =& -|\overline{\mathcal{M}}_{eq\to\nu q'}|^2\,, \qquad \text{(A15)} \\
|\overline{\mathcal{M}}_{eq_L\to\nu q'}|^2 =& -|\overline{\mathcal{M}}_{eq\to\nu q'}|^2\,, \qquad \text{(A16)} \\
|\overline{\mathcal{M}}_{e_L q_L\to\nu q'}|^2 =& |\overline{\mathcal{M}}_{eq\to\nu q'}|^2\,, \qquad \text{(A17)}
\end{aligned}
$$

The unpolarized-electron and polarized-electron matrix elements are related to each other in Eqs. A16 through A17 due to the $(1-\lambda_e)$ factor in the leptonic tensor. Consequently, one obtains the following relations between the structure functions:

$$
\begin{aligned}
F_{LU} =& -F_{UU} \qquad \text{(A18)} \\
F_{LL} =& -F_{UL} \qquad \text{(A19)} \\
F_{LT}^{\cos(\phi_q-\phi_{S_A})} =& -F_{UT}^{\cos(\phi_q-\phi_{S_A})} \qquad \text{(A20)} \\
F_{LT}^{\sin(\phi_q-\phi_{S_A})} =& -F_{UT}^{\sin(\phi_q-\phi_{S_A})} \qquad \text{(A21)}
\end{aligned}
$$

Appendix B: Hadron distribution inside jet

For unpolarized final-hadron state, one has TMD JFFs $\mathcal{D}_1$, $\mathcal{H}_1^{\perp}$ at leading-twist [9]:

$$
\begin{aligned}
\Delta(z_h,\vec{j}_\perp) =& \mathcal{D}_1^{h/q}(z_h,\vec{j}_\perp^2)\frac{\not{n}_-}{2} \\
&+ i\mathcal{H}_1^{\perp,h/q}(z_h,\vec{j}_\perp^2)\frac{\not{j}_\perp}{z_h M_h}\frac{\not{n}_-}{2}\,, \qquad \text{(B1)}
\end{aligned}
$$

The traces of the correlator are

$$
\begin{aligned}
\Delta^{h/q[\gamma^-]} =& \mathcal{D}_1^{h/q}(z_h,\vec{j}_\perp^2)\,, \qquad \text{(B2)} \\
\Delta^{h/q[i\sigma^{i-}\gamma_5]} =& \frac{\epsilon_T^{ij} j_\perp^j}{z_h M_h}\mathcal{H}_1^{\perp,h/q}(z_h,\vec{j}_\perp^2)\,, \qquad \text{(B3)}
\end{aligned}
$$

For an electron colliding with an unpolarized or a longitudinally polarized initial proton, one has the same partonic scattering amplitudes as shown in App. A. However, if the electron collides with a transversely polarized quark from the initial proton, the corresponding term in the hadronic tensor is given by

$$
H^{\mu\nu}_{\mathcal{H}_1^{\perp h/q}} = {\rm Tr}\left[\frac{\not{j}_\perp}{z_h M_h}\hat{\not{P}}_C\gamma^\mu\left(\frac{1-\gamma_5}{2}\right)\not{\phi}\hat{\not{P}}_A\gamma^\nu\left(\frac{1-\gamma_5}{2}\right)\right] \qquad \text{(B4)}
$$

where $\hat{P}_A = xP_A$ and $\hat{P}_C = P_C/z_h$. For different TMD-PDFs, the vector $\not{\phi}$ is $\left(-\not{S}_T\gamma_5\right)$ for h_1, $\left(-\lambda_p\not{k}_T\gamma_5/M\right)$ for $h_{1L}^{\perp}$, $\left(-i\not{k}_T/M\right)$ for $h_1^{\perp}$ and $\left((\vec{k}_T\cdot\vec{S}_T\not{k}_T - \vec{k}_T^2\not{S}_T/2)\gamma_5/M^2\right)$ for $h_{1T}^{\perp}$.

Note that there are three γ's between the $\left(\frac{1-\gamma_5}{2}\right)$'s in the hadronic tensor (Eq. B4), namely one always has

$$
\begin{aligned}
&\left(\frac{1-\gamma_5}{2}\right)\gamma_\alpha\gamma_\beta\gamma_\rho\left(\frac{1-\gamma_5}{2}\right) \\
&= \gamma_\alpha\gamma_\beta\gamma_\rho\left(\frac{1+\gamma_5}{2}\right)\left(\frac{1-\gamma_5}{2}\right) = 0\,. \qquad \text{(B5)}
\end{aligned}
$$

Therefore the expression in Eq. B4 vanishes. Consequently, contributions from transversely polarized quark

scattering with W-boson exchange does not exist. Therefore, all contributions related to the chiral-odd Collins jet-fragmentation function should not appear in the differential cross section for hadron-in-jet production with charged-current weak interaction. Below we show the differential cross section in terms of non-zero structure functions,

$$\begin{aligned}\frac{d\sigma^{ep\to\nu+\mathrm{jet}X}}{dy_J d^2p_{JT} d^2q_T dz_h d^2j_\perp} &= F^h_{UU} + \lambda_p F^h_{UL} \\ &+ |S_T| \Big[\cos(\phi_q-\phi_{S_A}) F_{UT}^{h,\cos(\phi_q-\phi_{S_A})} \\ &\quad + \sin(\phi_q-\phi_{S_A}) F_{UT}^{h,\sin(\phi_q-\phi_{S_A})}\Big] \\ &+ \lambda_e \Big[F^h_{LU} + |S_T|\sin(\phi_q-\phi_{S_A}) F_{LT}^{h,\sin(\phi_q-\phi_{S_A})} \\ &\quad + \lambda_p F^h_{LL} + |S_T|\cos(\phi_q-\phi_{S_A}) F_{LT}^{h,\cos(\phi_q-\phi_{S_A})})\Big] .\end{aligned} \tag{B6}$$

with 8 terms in total, where the structure functions are defined as below

$$\begin{aligned}F^h_{UU} =& \sum \frac{|\overline{\mathcal{M}}_{eq\to\nu q'}|^2}{16\pi^2\hat{s}^2} H(Q,\mu)\mathcal{D}_1(p_T^{\rm jet}R,\mu) \\ &\times \int \frac{b_T db_T}{2\pi} J_0(q_T b_T) f_1^{\rm TMD}(x,b_T,\mu) \\ &\times S_q(b_T, y_{\rm jet}, R, \mu)\,, \\ =& \mathcal{C}^h\left[f_1\mathcal{D}_1\right]_{eq\to\nu q'}\,,\end{aligned} \tag{B7}$$

$$F^h_{LU} = \mathcal{C}^h\left[f_1\mathcal{D}_1\right]_{e_L q\to\nu q'}\,, \tag{B8}$$

$$F^h_{UL} = \mathcal{C}^h\left[g_{1L}\mathcal{D}_1\right]_{eq_L\to\nu q'}\,, \tag{B9}$$

$$F^h_{LL} = \mathcal{C}^h\left[g_{1L}\mathcal{D}_1\right]_{e_L q_L\to\nu q'}\,, \tag{B10}$$

$$\begin{aligned}F_{UT}^{h,\cos(\phi_q-\phi_{S_A})} =& \sum \frac{|\overline{\mathcal{M}}_{eq_L\to\nu q'}|^2}{16\pi^2\hat{s}^2} H(Q,\mu)\mathcal{D}_1(p_T^{\rm jet}R,\mu) \\ &\times \int \frac{b_T^2 db_T}{4\pi M} J_1(q_T b_T) g_{1T}^{(1),\rm TMD}(x,b_T,\mu) \\ &\times S_q(b_T, y_{\rm jet}, R, \mu)\,, \\ =& \tilde{\mathcal{C}}^h\left[g_{1T}\mathcal{D}_1/M\right]_{eq_L\to\nu q'}\,,\end{aligned} \tag{B11}$$

$$F_{LT}^{h,\cos(\phi_q-\phi_{S_A})} = \tilde{\mathcal{C}}^h\left[g_{1T}\mathcal{D}_1/M\right]_{e_L q_L\to\nu q'}\,, \tag{B12}$$

$$F_{UT}^{h,\sin(\phi_q-\phi_{S_A})} = \tilde{\mathcal{C}}^h\left[f_{1T}^\perp\mathcal{D}_1/M\right]_{eq\to\nu q'}\,, \tag{B13}$$

$$F_{LT}^{h,\sin(\phi_q-\phi_{S_A})} = \tilde{\mathcal{C}}^h\left[f_{1T}^\perp\mathcal{D}_1/M\right]_{e_L q\to\nu q'}\,, \tag{B14}$$

We obtain relations between the hadron-in-jet structure functions similar to those for the inclusive-jets ones (see App. A):

$$F^h_{LU} = -F^h_{UU} \tag{B15}$$

$$F^h_{LL} = -F^h_{UL} \tag{B16}$$

$$F_{LT}^{h,\cos(\phi_q-\phi_{S_A})} = -F_{UT}^{h,\cos(\phi_q-\phi_{S_A})} \tag{B17}$$

$$F_{LT}^{h,\sin(\phi_q-\phi_{S_A})} = -F_{UT}^{h,\sin(\phi_q-\phi_{S_A})} \tag{B18}$$